



Oxygen Enrichment for High Mach Number Scramjets

Nicholas N. Gibbons, Vincent Wheatley1

Abstract

Oxygen enrichment is the addition of small amounts of gaseous oxygen to the fuel of a hypersonic vehicle, to promote vigorous combustion and prevent extinction in difficult conditions. In this work, a preliminary numerical study has been performed to evaluate the prospects of using oxygen enrichment in high Mach number Scramjets, the kind developed for access to space, where the engine must operate through a large range of Mach numbers and atmospheric conditions. A previously published flowpath, the Mach 12 REST scramjet, has been chosen as a baseline geometry, and simulated with and without oxygen enrichment at conditions matching an experimental tunnel test. These numerical simulations are performed using the University of Queensland's compressible flow solver Eilmer, which uses a Jacobian-Free Newton-Krylov approach to solve the steady-state, reacting, Reynolds-Averaged Navier-Stokes equations on an unstructured, hexahedral grid in a highly parallel fashion. The results show good agreement with the experiments in the cases with no oxygen enrichment, and encouraging improvements in the combustion behaviour with added oxygen. In addition, we present the development of a quasi-1D meta-model of the flowpath that can be used for systems-level studies of oxygen enrichment that are planned for future work.

Keywords: Hypersonics, Combustion, Computational Fluid Dynamics

1. Introduction

Flying to space with an air-breathing propulsion system is a challenging engineering problem. Chiefly, the difficulty in designing such a propulsion system comes from the wide range of Mach numbers that it must operate through, from ignition at around Mach 5 to final shutdown at Mach 10 or above. An engine shape that is optimised for either trajectory point would be inoperable at the other end of the flight, and so compromises must be made that impact the performance at both extremes.

Despite the challenges, a successful conceptual design of such a system is presented in Ref. [1], which uses numerical simulations of a subscale, 3D shape-transitioning scramjet engine to demonstrate net thrust at both ends of the trajectory, utilising the fuel jets to anchor a stable dual-mode combustion flowfield at low speeds, and transitioning to a fully supersonic flow with no struts or flameholders at high speeds.

This work builds on these results, in an attempt to improve the overall performance of such a system by utilising oxygen enrichment at the end of the trajectory, when the thrust margin is small and the potential for performance gains is largest. Oxygen enrichment is the mixing of a small amount of pure oxygen into the fuel of an air-breathing propulsion system [2], with the goal of improving ignition speed or combustion efficiency or both. Ultimately, the goal of this project is to see if oxygen enrichment allows an accelerating scramjet engine to reach higher altitudes or a faster final staging speed, but for this work we are focused on a first step: developing and validating a numerical simulation technique that includes oxygen enrichment. In this paper we will present preliminary calculations showing that our method can recover the results of experiments on an existing high Mach number scramjet, and then perform some nominal oxygen enrichment to explore its effects.

¹School of Mechanical and Mining Engineering, University of Queensland, St. Lucia QLD 4072, Australia

2. Numerical Method

Simulations have been conducted using the University of Queensland's open-source compressible flow code Eilmer [3]. In this work, we use the newly developed Jacobian-Free Newton-Krylov method [4], to solve the steady-state turbulent reacting Reynolds Averaged Navier Stokes (RANS) equations. These include a transport equation for each of the chemical species in the reaction mechanism (equation 1), three components of the momentum (equation 2), the total energy (equation 3), and the one-equation Spalart-Allmaras-Edwards turbulence model (equation 4).

$$\frac{\partial \rho_s}{\partial t} + \frac{\partial}{\partial x_j} (\rho_s u_j) + \frac{\partial}{\partial x_j} (v_{sj}) = \dot{\omega}_s \tag{1}$$

$$\frac{\partial}{\partial t}(\rho u_i) + \frac{\partial}{\partial x_j}(\rho u_j u_i) = -\frac{\partial p}{\partial x_i} + \frac{\partial \tau_{ji}}{\partial x_j}$$
 (2)

$$\frac{\partial}{\partial t}(E) + \frac{\partial}{\partial x_j}[(E+p)u_j] = \frac{\partial}{\partial x_j}(u_i t_{ij}) - \frac{\partial q_j}{\partial x_j}$$
(3)

$$\frac{\partial \rho \hat{\nu}}{\partial t} + \frac{\partial \rho \hat{\nu} \tilde{u}_{j}}{\partial x_{j}} = \rho c_{b1} (1 - f_{t2}) \hat{S} \hat{\nu} - \rho \left[c_{w1} f_{w} - \frac{c_{b1}}{\kappa^{2}} f_{t2} \right] \left(\frac{\hat{\nu}}{d} \right)^{2} + \frac{1}{\sigma} \frac{\partial}{\partial x_{j}} \left(\rho (\nu + \hat{\nu}) \frac{\partial \hat{\nu}}{\partial x_{j}} \right) + \frac{c_{b2}}{\sigma} \rho \frac{\partial \hat{\nu}}{\partial x_{i}} \frac{\partial \hat{\nu}}{\partial x_{i}}$$

$$(4)$$

These equations are solved by first discretising the set of partial differential equations onto a mesh or grid of finite-volume elements, resulting in an integral form where the change in a vector of conserved variables \mathbf{U} is affected by the combination of convective and viscous fluxes (\mathbf{F}^c and \mathbf{F}^v) flowing through each interface, and also the integral of the source terms \mathbf{Q} throughout the cell's volume.

$$\frac{\partial \mathbf{U}}{\partial t} = -\frac{1}{\mathcal{V}} \sum_{f} [(\mathbf{F}_{fj} - \mathbf{V}_{fj}) n_{fj} S_f] + \mathbf{S}$$
 (5)

In this work, the inviscid fluxes **F** are computed with the upwinding scheme of Ref. [5], and the viscous terms are computed using a weighted-least squares method at cell centers and then transferred to each face using the averaging method of Ref. [6]. Ref. [3] should be consulted for further details.

2.1. Steady-State Solver

Together, the terms on the right-hand side of Equation 5 can be collected into a vector called the residual **R**

$$\frac{\partial \mathbf{U}}{\partial t} = \mathbf{R} \tag{6}$$

Simply calculating the residual and numerically integrating Equation 5 gives a simple explicit scheme that is first order accurate in time. However, for steady-state problems it is far more efficient to derive a Newton's method-like scheme that seeks a solution to $\mathbf{R}=0$ via a series of implicit pseudo-timesteps. The method is conceptually similar to the Backward-Euler scheme, where the change in conserved variables from timestep n to timestep n+1 is evaluated using the residual vector at n+1. Since \mathbf{R}^{n+1} is not known, it is related to the conserved quantities using a first order linearisation.

$$\left[\frac{1}{\Delta t}\mathbf{I} - \frac{\partial \mathbf{R}}{\partial \mathbf{U}}^n\right] \Delta \mathbf{U}^n = \mathbf{R}^n$$
 (7)

An exact solution of this matrix would be expensive and is not generally necessary since convergence can be achieved as long as $|\mathbf{R}^{n+1}| < |\mathbf{R}^n|$. Instead the Generalized Minimal Residual (GMRES) method is used to solve the matrix problem iteratively, utilising Fréchet derivatives to avoid having to actually

construct the full Jacobian matrix $\partial \mathbf{R}/\partial \mathbf{U}$. These derivatives are evaluated using a complex step finite-difference method that perturbs each conserved variable in the complex plane and divides the imaginary component of the recalculated \mathbf{R} vector by the size of the perturbation.

$$\frac{\partial \mathbf{R}_i}{\partial \mathbf{U}_i} = \frac{Im(R_i(U_j + ih))}{h} \tag{8}$$

This approach results in a nearly exact derivative that is robust to choice of h, and avoids having to manually differentiate the residual vector call chain and every function therein. This combination of methods has been dubbed the Jacobian-Free Newton-Krylov (JFNK) approach, and much more detail on the implementation and testing of Eilmer's JFNK can be found in Ref. [4].

3. Problem Description

This paper considers numerical simulations of the Mach 12 REST (Rectangular-to-Elliptical Shape Transitioning) flowpath. The M12REST was developed for accelerating access to space applications by Ref. [7] and went through subsequent refinements and experimental testing by Ref. [8], Ref. [9], and Ref. [10]. A schematic depiction of the inlet is shown in figure 1, showing the centreplane shape with cross sections of the flowpath beneath.

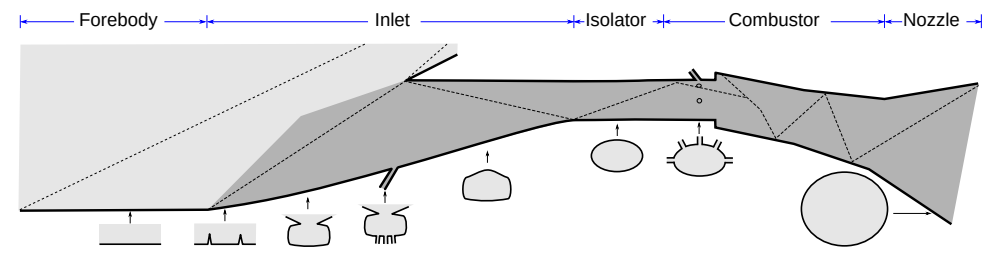


Fig 1. Mach 12 REST Inlet Tunnel Model Geometry (Not to Scale).

Hydrogen fuel is injected on the inlet through three 2 mm diameter injectors, and also in the elliptical combustor through five 1.6 mm diameter injectors.

The actual geometry that is simulated is a wind-tunnel scale model build for experimental testing. It includes a long flat plate forebody that would not be present in a flight vehicle, and also a placeholder nozzle at the end of the combustor that is not designed to maximise thrust. The experiments of interest were performed by Ref. [9] in the University of Queensland's T4 shock tunnel in December 2013. Two specific tests are of interest, first an unfuelled shot (no. 11486), and a fuelled shot, (no. 11491) with an equivalence ratio of 1.24. The flow coming out of the facility nozzle in each case has been computed by Ref. [9], shown below in table 1. Note that because of dissociation in the stagnation region of the facility, these conditions contain a significant amount of NO, approximately 8% by mass. This NO is effectively inert, though it does reduce the amount of available oxygen in the incoming freestream. Accordingly, the equivalence ratio of 1.24 is calculated using only the O and O_2 that remains.

Type	Test	p (Pa)	T (K)	u (m/s)	М	H_t (MJ/kg)	NO wt%	Eqv. Ratio
No Fuel	11486	1131.3	382.5	3615.0	9.2	6.95	8.3	0.0
Fuel	11491	1176.6	386.8	3630.2	9.1	7.01	8.3	1.24

Table 1. Flowpath inflow conditions from Ref. [9], Appendix E

4. Experimental Validation

A rendering of the solved 3D flowfield is shown in figure 2. This shows the solid surfaces of the shape-transitioning inlet in grey, with five slices of Mach number showing the progression of the shock structure as the flow moves downstream. The green clouds are a 3D volume-rendering of the fuel mass fraction,

made visible using an opacity mask that makes small values of the H_2 mass fraction transparent. Similarly, the product species H_2O is shown in an yellow/orange/red volume rendering, which shows where combustion has occurred.

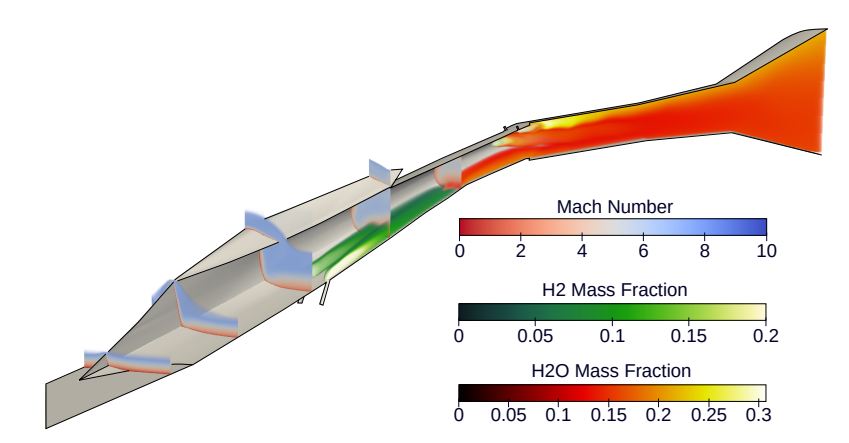


Fig 2. Three-dimensional volume rendering of the simulated flowfield.

The experimental data collected by Ref. [9] consists of a series of pressure measurements taken by sensors on the walls of the flowpath. These sensors were placed on the centreline of the flowpath on both the body side (downward in figure 2). We can compare the pressure predicted by the CFD solution to these measurements, which has been done in figure 3 below.

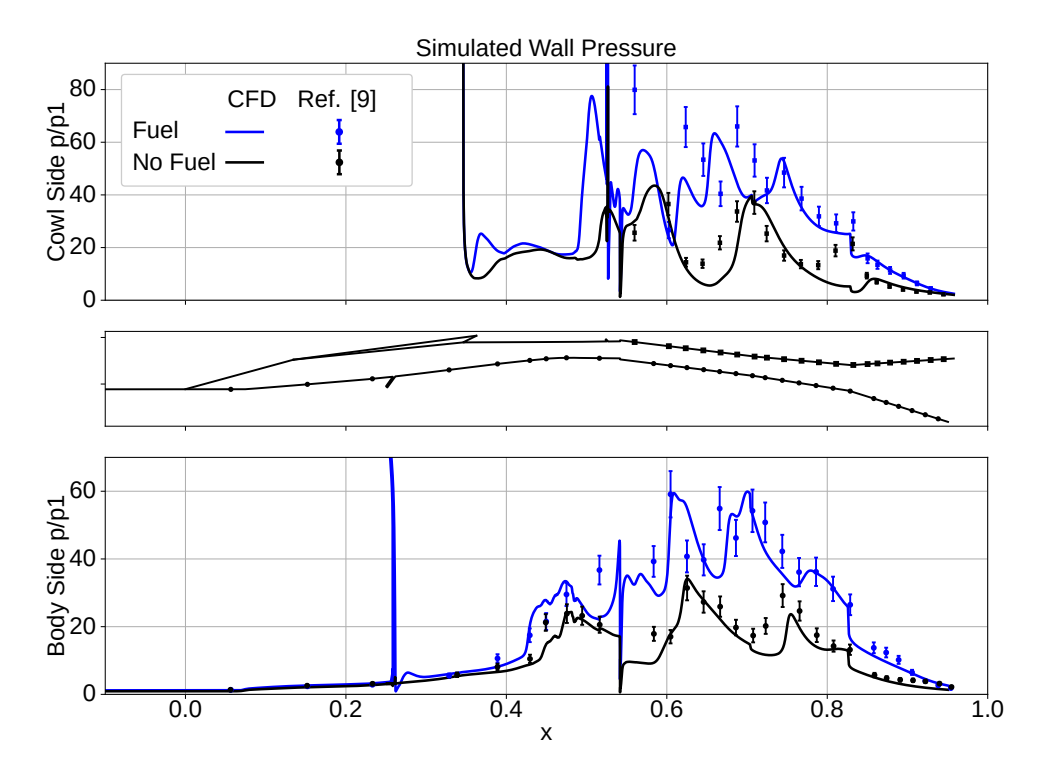


Fig 3. Wall pressure predicted by the CFD compared to experiments.

These figures show the normalised pressure p/p_1 , which is pressure at a given x location divided by the pressure measured at the first measurement location on the forebody. Normalising is necessary to

deal with the fact that the experimental conditions are not perfectly steady, and change slowly over the amount of time that the gas takes to pass through the flow path. The bottom figure shows the body side pressure, measured at the positions noted by small circles in the middle figure. Agreement is fairly good here, especially with the unfuelled case which matches very well. The top figure shows the cowl side pressure measured at the small squares. Agreement here is not quite as good, especially for the fuelled case, which has some errant sensors at the combustor entrance, but the overall results are similar in accuracy to the simulations in Ref. [9] and Ref. [10], which were performed with a different CFD code. Given the level of uncertainty involved with shock tunnel experiments and the complexity of the flowfield and the physics being simulated, these results are sufficient to validate the methodology in this paper for a preliminary conceptual study.

5. Quasi-1D CFD Results

In order to further analyse the CFD results, this section develops a method for reducing the 3D flowfield data into a quasi-1D field that varies only in the streamwise direction. This method proceeds by taking a number slices that march down the flowpath, and then computes the total flux of mass, momentum, and energy passing through each slice. The basic idea is illustrated in figure 4.

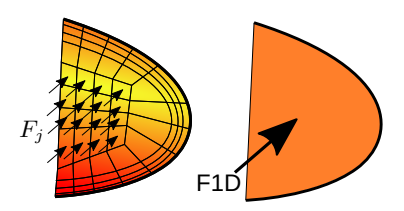


Fig 4. Illustration of one-dimensionalisation process.

For each slice the method then determines a single flowstate that, if put through the total area of the slice, would produce the same mass, momentum, and energy total flux as the CFD. These totals are calculated using equations 9, which sum over all of the cell faces j in the slice. The velocity u_j used is the component in the direction normal to the slice.

$$F_{mass} = \sum_{j} \sum_{s} \rho_{sj} u_j A_j \quad F_{mom} = \sum_{j} (\rho_j u_j^2 + p_j) A_j \quad F_{energy} = \sum_{j} u_j (\rho_j E_j + p_j) A_j$$
 (9)

To determine a single flowstate that matches these fluxes, we must iteratively solve a non-linear equation that is implicit in the temperature T, an equation that is constructed from the expression for the total energy as follows.

$$0 = \sum_{s} F_{s} e_{s}(T) + \frac{1}{2} F_{mass} \left[\frac{F_{mom} + \sqrt{F_{mom}^{2} - 4F_{mass}^{2}RT}}{2F_{mass}} \right]^{2} + F_{mass}RT - F_{energy}$$
 (10)

With the temperature known the velocity can be deduced by solving equation 11, derived from the momentum equation and equation of state.

$$v = \frac{F_{mom} + \sqrt{F_{mom}^2 - 4F_{mass}^2 RT}}{2F_{mass}}$$
 (11)

The rest of the flow state is then reconstructed by using equations 12, which are derived from the mass flux expression.

$$\rho = F_{mass}/v \qquad p = F_{mass}/vRT \qquad Y_s = \frac{\sum_j \rho_{sj} u_j}{F_{mass}} \tag{12}$$

A major complication to this procedure occurs in the part of the flowfield upstream of the cowl closure notch. These slices contain gas which does not pass into the engine, exiting through the outflow boundaries on the outside of the inlet, which invalidates the assumption of quasi-1D flow and would make them not comparable with the flowstates estimated downstream. To handle this problem, the postprocessing script performs stream-tracing from each of the cells in each slice that is upstream of the cowl closure point, and excludes any cells from the sum j that are projected to not be captured by the inlet. This introduces a small amount of noise to these flowstate estimates that is generally not an issue.

An example of the Q1D flow results, for the unfuelled, fuelled, and enriched configurations, is shown in figure 5. This enriched configuration uses an identical computational setup as the fuelled case used for the validation exercise, except with a nominal amount of pure oxygen premixed into the five combustor fuel injectors. In this instance, we have chosen an equal mass flow rate to the hydrogen $\dot{m}_{O2}=\dot{m}_{H2}$, as an arbitrary but reasonable first benchmark.

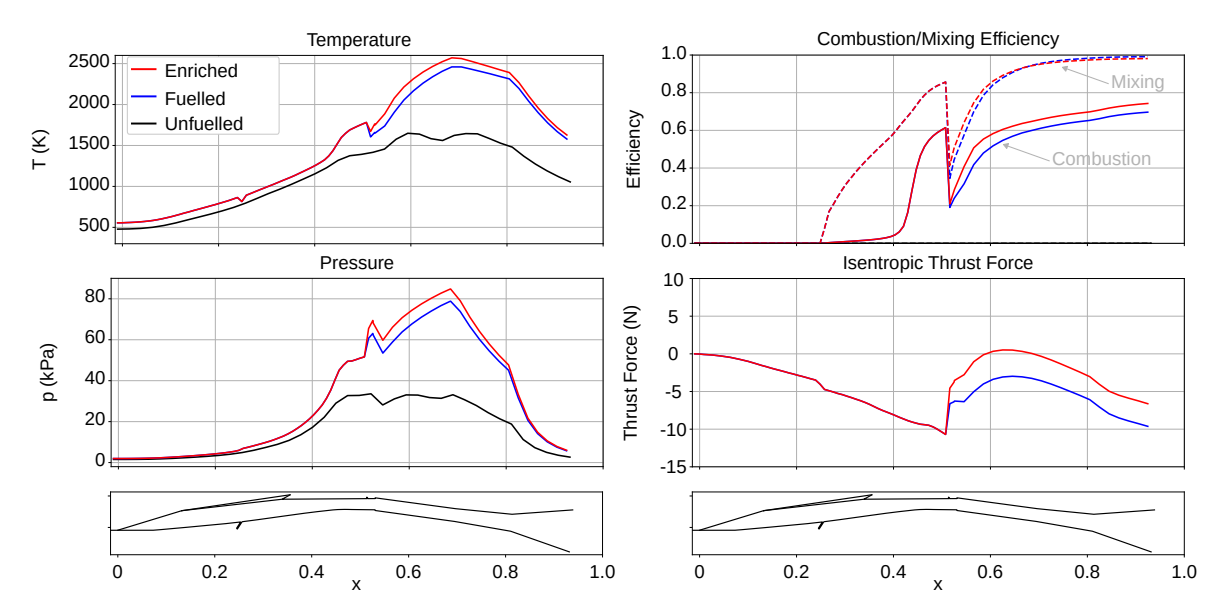


Fig 5. Q1D pressure, temperature, mixing/combustion efficiency, and isentropic thrust force.

The left hand subplots of figure 5 display the pressure and temperature at each streamwise station. The effect of combustion is clearly visible, note the increase of both quantities over the unfuelled case. Also visible is a spike in the pressure at around x=0.5 where fuel is injected, and a sharp dip just downstream of this point, where the combustor area expands. But the two most interesting results are shown on the right-hand column of subplots. The first of these is a combined mixing and combustion efficiency, computed using the method of Ref. [11]. As one might expect, the addition of premixed oxygen produces a small but noticeable boost in the mixing efficiency, and a large and quite significant boost in combustion efficiency, the amount of fuel that is actually being reacting to completion.

Most interesting of all is the lower-right plot which shows quantity called the "Inviscid Thrust Force", or ITF, an estimate of the thrust produced by an ideal expansion of the gas at each point. It is calculated using equation 13, which introduces the stagnation pressure p_t , and the ambient pressure of the freestream air, assumed to be $p_{amb}=1511~{\rm Pa}$.

$$ITF = \dot{m} \sqrt{\frac{2\gamma RT}{\gamma - 1} \left[\frac{p_{amb}}{p} \right]^{\frac{\gamma - 1}{\gamma}} \left(\left[\frac{p_t}{p_{amb}} \right]^{\frac{\gamma - 1}{\gamma}} - 1 \right)}$$
 (13)

The lines in this figure have the ITF at the start of the flowpath subtracted off for visualisation purposes, so that they both begin at zero. Both curves decay through the inlet due to viscous losses as well

as total pressure losses from the compression waves. Some thrust potential is rapidly gained by the injection of fuel at x=0.55, and then more is recovered as the fuel burns, but the blue line shows that the overall peak is still below the initial amount. In other words, the unenriched engine does not produce net uninstalled thrust. (This result is unsurprising for a tunnel-scale, cold wall model, which has many effects working against it that would not be true in flight). However, with oxygen enrichment the peak net ITF is higher than the initial amount, demonstrating that oxygen enrichment does have significant potential for improving thrust performance, even in a small scale model where net thrust is difficult to achieve.

6. Preliminary Propulsion Meta-model Development

To evaluate whether the thrust improvement from oxygen enrichment is worth the associated weight and volume penalty of the oxygen tank, future systems-level analysis is planned that will simulate the trajectory of a candidate three-stage accelerating hypersonic vehicle. This analysis will require a model for the engine performance at different Mach numbers and fuelling conditions, including varying amounts of oxygen enrichment.

Although this model may be informed by CFD, systems analyses need to be fast and approximate, and certainly cannot be performing a 3D reacting CFD calculation at every timestep. Anticipating this, we have begun developing a physics-based surrogate model for supersonic flowpath performance that can be calibrated to a CFD simulation, packaged into a code called "swft". swft is based on a quasi-1D space-marching approach that solves the mass, momentum, and energy equations in a predetermined schedule of areas that march downstream. Each step considers a control volume defined as follows:

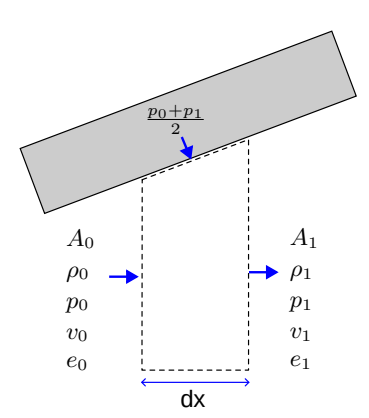


Fig 6. Control volume for a single instance of supersonic space marching.

Conservation of mass, momentum, and energy across this control volume can be written as follows.

$$\rho_0 v_0 A_0 = \rho_1 v_1 A_1 \tag{14}$$

$$(\rho_0 v_0^2 + p_0) A_0 = (\rho_1 v_1^2 + p_1) A_1 + \frac{p_0 + p_1}{2} dA + \tau \pi D dx$$
(15)

$$(\rho_0 E_0 + p_0) v_0 A_0 = (\rho_1 E_1 + p_1) v_1 A_1 + \dot{H} A dx \tag{16}$$

$$p_1 - \rho_1 R T_1 \tag{17}$$

For a small change dx the downstream quantities in the control volume can be defined as small differential changes from the upstream ones, for example: $\rho_1 = \rho + d\rho$. Performing these substitutions, and

then cancelling all higher order products of differentials, the equations can be reduced to the following linear system:

$$\rho v dA + A v d\rho + A \rho dv = 0 \tag{18}$$

$$\rho v^2 dA + Av^2 d\rho + 2A\rho v dv + \tau D dx + A dp = 0$$
(19)

$$Adv\rho v^{2} + ((Ade + EdA)\rho + dAp + AEd\rho + Adp)v + AEdv\rho + Advp - \dot{H}Adx = 0$$
 (20)

$$(\rho R)/c_v de + RTd\rho - dp = 0 \tag{21}$$

This system of equations is linear in the increments $d\rho$, dv, dp, and de (dA is known from the predetermined area schedule) and so it can be solved symbolically using a computer algebra program and used to iteratively march downstream from a known initial state. A trio of test runs of the solver is shown in figure 7, which verify the implementation against the analytic solutions for compressible flow with area change, heat addition, and friction respectively, which are taken from Ref. [12].

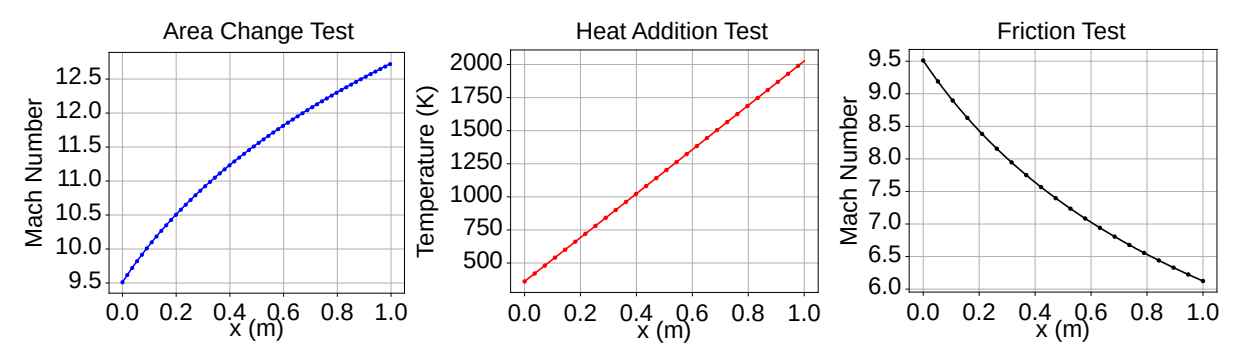


Fig 7. Verification tests for Q1D space marching solver.

Any actual flowpath will have a myriad of complexities that a quasi-1D solver will struggle to approximate in a predictive manner. Instead, the goal of this work is to calibrate the solver to a given simulation, or set of simulations, by using a numerical optimiser to adjust the simulation parameters until a known solution is matched. Principally, this consists of the friction factor f and heat-addition/heat-loss terms \dot{H} , which are allowed to vary in space throughout the flow. This friction factor is taken from Ref. [12] and is used to compute the shear stress τ in equation 15 as follows.

$$\tau = \frac{1}{8}f\rho v^2 \tag{22}$$

It follows then, that the Q1D solver should additionally report the total derivatives of the flow field with respect to these parameters. These derivatives could be calculated using some kind of finite-difference method, where they are perturbed one point at a time, but this approach is expensive for a large number of parameters and involves choosing a step size for the perturbations that can be difficult to generalise. Instead, the solver has been equipped with a novel method for computing the flowfield derivatives during the solution process, which is briefly described here.

We begin by collecting the primitive variables into a vector called $\mathbf{P}=[\rho,p,v,e]$ and the equations 14 - 17 into a vector called the residual, or $\mathbf{R}(\mathbf{P}_0,\mathbf{P}_1,f)$. The residual represents the conservation laws governing a single step in space, and a requirement for satisfying those laws is $\mathbf{R}=0$. Consider then, a differential change in \mathbf{R} .

$$d\mathbf{R} = \frac{\partial \mathbf{R}}{\partial \mathbf{P}_0} d\mathbf{P}_0 + \frac{\partial \mathbf{R}}{\partial \mathbf{P}_1} d\mathbf{P}_1 + \frac{\partial \mathbf{R}}{\partial f} df$$
 (23)

In this instance the friction factor f is a stand in for whatever input parameter we are interested in differentiating with respect to. Since we only care about the partial derivatives of the flow field, it is okay to consider these parameters one at a time. A crucial piece of insight into equation 23 is that, if we were to change the friction factor f, the space marching solver would ensure that the solution \mathbf{P}_1 preserves mass, momentum, and energy, that is to say that $\mathbf{R}=0$ even if f changes. On the left hand side then, we are able to set \mathbf{dR} to zero, and if we consider the very first control volume in the space marching, we may also say that \mathbf{dP}_0 is zero as well, since the initial condition is fixed. Therefore we may rearrange equation 23 to get the following.

$$\frac{\partial \mathbf{R}}{\partial \mathbf{P}_1} \frac{\mathbf{dP}_1}{df} = -\frac{\partial \mathbf{R}}{\partial f} \tag{24}$$

This is a very interesting result. The right hand side is a vector of partial derivatives of the residual with respect to the parameter f, which can be computed quite easily by differentiating equation 15. On the left hand side we have a matrix vector product, firstly the Jacobian matrix, which is known, and secondly a vector of total derivatives of the flowstate \mathbf{P}_1 with respect to the parameter of interest f. These total derivatives are what is needed for an optimiser to do its work, and this expression allows us to calculate them using a straightforward linear system solution. Since the matrix in question is a 4x4 with comparatively simple expressions, these are also computed using a symbolic algebra program. An example of the total derivatives with equation 24, compared to a finite-difference estimate made by subtracting two simulations with slightly different f parameters, is shown in figure 8. Agreement is good enough that the two lines are visually identical.

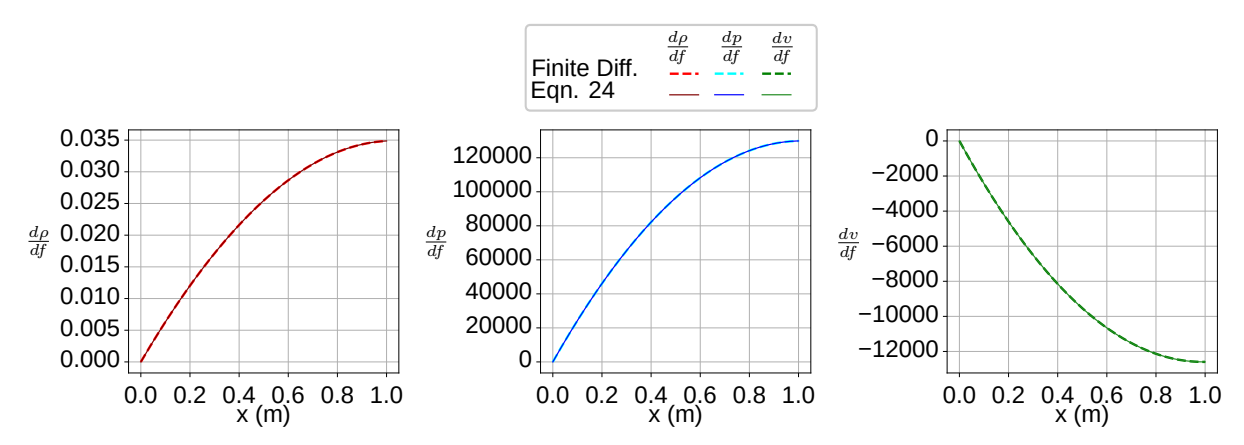


Fig 8. Total Derivatives vs. Finite Difference with respect to friction factor f.

A complication to this process is that once we move past the first control volume in the domain, it is no longer true that \mathbf{dP}_0 is equal to zero. Additionally, the solution \mathbf{P}_1 is not just dependent on f in this control volume, but also is affected by the value of f in all prior ones, an effect which is quite important when considering non-uniform distributions of f. These considerations lead to a significantly more complex version of the total derivative formulation, which for control volume i in the sequence, can be written as follows:

$$d\mathbf{R}_{i} = \frac{\partial \mathbf{R}_{i}}{\partial \mathbf{P}_{i-1}} \left[\sum_{j}^{i-1} \frac{d\mathbf{P}_{i-1}}{df_{j}} \right] + \frac{\partial \mathbf{R}_{i}}{\partial \mathbf{P}_{i}} d\mathbf{P}_{i} + \frac{\partial \mathbf{R}_{i}}{\partial f_{i-1}} df_{i-1}$$
(25)

Setting $dR_i = 0$ as before, we can consider the different values of f_i to be independent, allowing us to focus on a single df_i by setting all others to zero. For a control volume of interest i then, we begin

at the first control volume j=0 and solve the following matrix expression for each value of j moving downstream until we reach j=i-1.

$$\frac{\partial \mathbf{R}_i}{\partial \mathbf{P}_i} \frac{\mathbf{dP}_i}{df_j} = -\frac{\partial \mathbf{R}_i}{\partial \mathbf{P}_{i-1}} \frac{\mathbf{dP}_{i-1}}{df_j}$$
(26)

Note that the previous control volume's total derivatives \mathbf{dP}_{i-1}/df_j are known from the previous step. Eventually, when we reach the control volume i, we solve essentially the same equation as in the simpler case, which is repeated here with the new index notation added.

$$\frac{\partial \mathbf{R}_i}{\partial \mathbf{P}_i} \frac{\mathbf{dP}_i}{df_{i-1}} = -\frac{\partial \mathbf{R}_i}{\partial f_{i-1}} \tag{27}$$

This process creates a lower triangular matrix of total derivatives that grows in size with each step of the calculation, with one dimension spanning the flowfield values ${\bf P}$ and the other the friction factors at each point in space f_j . The matrix is lower triangular because each point in the flowfield is only affected by the friction factors upstream of it, as the flow in swft is always supersonic. This matrix has been used to guide an a numerical optimiser that attempts to fit a Q1D simulation to the 1D reduced unfuelled CFD results presented in the earlier section. A schedule of 24 linearly interpolated friction factors and a single constant heat loss rate \dot{H} was used, along with the SLSQP optimiser available in scipy's minimize routine. The objective function was the L2 norm of the error in Mach number, and 197 iterations was sufficient to converge to the result in figure 9.

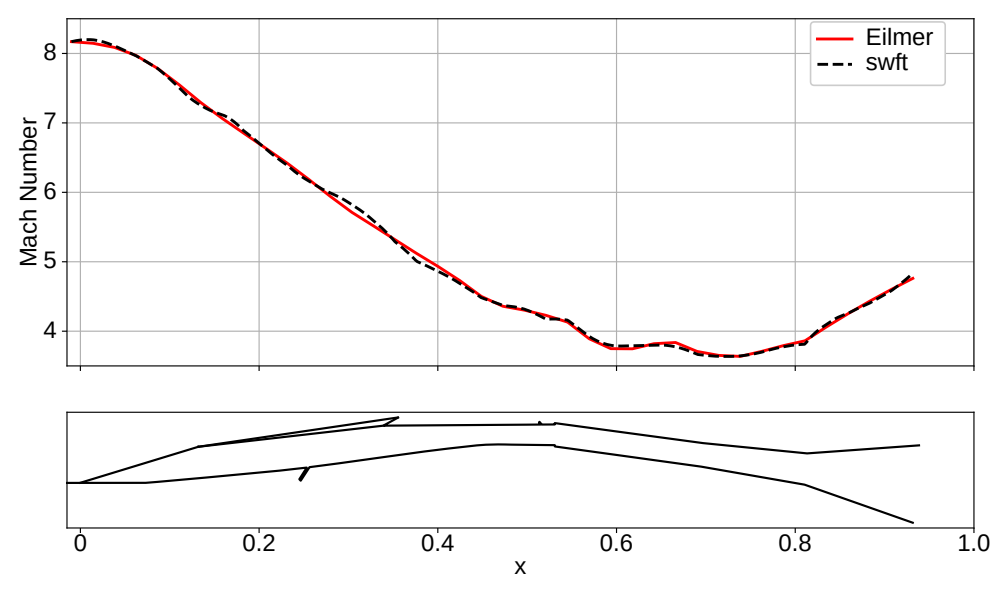


Fig 9. Optimised space-marching code "swft" against unfuelled result from CFD.

The result shows that the space marching solver is able to capture the variation in Mach number through the flowpath fairly well, including some of the complex behaviour in the combustor where there are shocks and expansion waves. The optimisation process takes about 8 seconds on a desktop PC, and the Q1D solver evaluates extremely fast, on the order of milliseconds, so it is perfectly suitable for systems-level analysis where rapid evaluation is needed. An additional bonus is that the framework for differentiating the outputs of the solver is extremely useful in *co-design* [13], where the vehicle control and geometry are optimised at the same in the same loop. Future work will explore the effect of differentiable flow solvers in aiding this approach.

7. Conclusions

This paper has presented a preliminary study into the prospects of oxygen enrichment for enhancing the performance of high mach number scramjets. We have presented numerical simulations of an existing flowpath, the Mach 12 REST engine, performed using the University of Queensland's open-source compressible flow code Eilmer, which have lead to three main conclusions.

Firstly, we have validated the numerical simulations against a wind-tunnel scale model that was tested by Ref. [9]. Specifically, the wall pressure measured in the unfuelled case is matched very well, while the agreement with the fuelled, reacting case is on par with past work using different codes. This is important because this work is the first attempt to solve a reacting RANS flowfield of this level of complexity using Eilmer. As to the reason for the reacting field being more difficult to match than the non-reacting one, the level of uncertainty in shock-tunnel experiments is currently too high to be sure exactly why this is. More experiments with longer steady test time would likely be the best course of action to answer this issue.

Secondly, we have shown that using a nominal amount of oxygen enrichment yields a significant improvement in uninstalled thrust force, raising the peak value from slightly negative to slightly positive. This result was not necessarily a forgone conclusion. Previous studies into modifying the M12REST's fuelling scheme, such as Ref. [10], have sometimes observed overheating in the combustor and other diminishing returns that have hindered performance in addition to the helpful effects from the modification. This work has shown that oxygen enrichment does not result in overheating, at least in this configuration.

Finally, this work has taken the first steps toward developing a novel, fast, meta-model for the propulsion system that can be applied to a systems level analysis of the benefits of oxygen enrichment. This model is based on a quasi-1D solution of the supersonic, compressible flow equations with wall friction and heat addition. In addition to producing a quasi-1D flowfield the solver has been equipped with routines for computing flow derivatives with respect to the input parameters, based on a novel total derivative method that is presented here for the first time. This method allows the solver to be tuned or fitted to a set of CFD results, though it is known yet how well this tuning can be applied away from the set of conditions the model is tuned for. Additionally, only an unfuelled test case has so far been considered. Test cases with reactions on will be a part of future work.

References

- [1] D. Curran, V. Wheatley, and M. Smart, "High mach number operation of accelerator scramjet engine," Journal of Spacecraft and Rockets, vol. 60, no. 3, pp. 884–898, 2023.
- [2] A. Rudakov and V. Krjutchenko, "Additional fuel component application for hydrogen scramjet boosting," in Aerospace Atlantic Conference & Exposition, no. 900990, 1990.
- [3] N. N. Gibbons, K. A. Damm, P. A. Jacobs, and R. J. Gollan, "Eilmer: An open-source multi-physics hypersonic flow solver," Computer Physics Communications, vol. 282, no. 108551, 2023.
- [4] K. A. Damm, N. N. Gibbons, and R. Gollan, "Application of a jacobian-free newton-krylov method to the simulation of hypersonic flows," in AIAA SCITECH 2023 Forum, no. 2023-2295, January 2023.
- [5] D. Haenel, R. Schewane, and G. Seider, "On the accuracy of upwind schemes for the solution of the navier-stokes equations," in 8th Computational Fluid Dynamics Conference, no. 1105, (Honolulu, HI, USA), June 1987.
- [6] A. Haselbacher and J. Blazek, "Accurate and efficient discretization of navier-stokes equations on mixed grids," AIAA Journal, vol. 38, pp. 2094–2102, November 2000.
- [7] M. V. Suraweera and M. K. Smart, "Shock-tunnel experiments with a mach 12 rectangular-to-elliptical shape-transition scramjet at offdesign conditions," *Journal of Propulsion and Power*, vol. 25, no. 3, pp. 555–564, 2009.
- [8] D. Wise, Experimental investigation of a three dimensional scramjet engine at hypervelocity conditions. PhD thesis, The University of Queensland, School of Mechanical and Mining Engineering, St Lucia, QLD 4072, 2015.
- [9] J. E. Barth, Mixing and Combustion Enhancement in a Mach 12 Shape-Transitioning Scramjet Engine. PhD thesis, The University of Queensland, School of Mechanical and Mining Engineering, St Lucia, QLD 4072, 2014.
- [10] W. O. Landsberg, Improving Performance of High Mach Number Scramjets: Fuelling Strategies and Combustor Design. PhD thesis, The University of Queensland, School of Mechanical and Mining Engineering, St Lucia, QLD 4072, 2018.
- [11] N. N. Gibbons, Simulation and Dynamics of Hypersonic Combustion. PhD thesis, The University of Queensland, School of Mechanical and Mining Engineering, St Lucia, QLD 4072, 2019.
- [12] F. White, Fluid Mechanics. McGraw Hill, seventh edition ed., 2010.
- [13] A. Lock, G. Oberman, I. H. Jahn, C. van der Heide, V. Bone, P. M. Dower, and C. Manzie, "Hypersonic glide vehicle shape and trajectory co-design," in AIAA SCITECH 2025 Forum, no. 2025-1337, January 2025.